arXiv:1011.3043v1 [cond-mat.mes-hall] 12 Nov 2010

# Irradiated bilayer graphene

**D. S. L. Abergel[1,2] and Tapash Chakraborty[2]**

[1] Condensed Matter Theory Center, University of Maryland, College Park, MD USA 20742.

[2] Department of Physics and Astronomy, University of Manitoba, Winnipeg, MB, Canada, R3T 2N2.

PACS numbers: 73.22.Pr, 78.67.Wj

**Abstract.** We describe the gated bilayer graphene system when it is subjected to intense terahertz frequency electromagnetic radiation. We examine the electron band structure and density of states via exact diagonalization methods within Floquet theory. We find that dynamical states are induced which lead to modification of the band structure. We first examine the situation where there is no external magnetic field. In the unbiased case, dynamical gaps appear in the spectrum which manifest as dips in the density of states. For finite interlayer bias (where a static gap is present in the band structure of unirradiated bilayer graphene), dynamical states may be induced in the static gap. These states can show a high degree of valley polarization. When the system is placed in a strong magnetic field, the radiation induces coupling between the Landau levels which allows dynamical levels to exist. For strong fields, this means the Landau levels are smeared to form a near-continuum of states.

## 1. Introduction

Graphene [1] and its bilayer [2] have attracted much attention recently due to the novel fundamental physics that they display and huge scope that they have for device applications [3, 4]. In particular, electrons in monolayer graphene (whose low-energy quasiparticles mimic chiral Dirac fermions with linear dispersion) have displayed relativistic-like phenomena, including Klein tunneling [5, 6] and the half-integer quantum Hall effect [7, 8]. Electrons in bilayer graphene show properties which are hybrid between the monolayer and traditional two-dimensional semiconductor systems, since the low-energy quasiparticles are chiral, but the inter-layer coupling induces an effective mass and corresponding quadratic energy dispersion. A fully-tunable gap can be opened at the charge neutrality point by application of a transverse electric field (either by gating [9] or by doping [2]), a feature which is unique to this system.

Monolayer graphene which is irradiated by monochromatic, high-intensity laser light has been studied theoretically for the bulk [10, 11, 12, 13, 14, 15], in nanoribbons [16, 17], and in *np*-junctions [18, 19]. Experimental investigations of few-layer graphene have also been carried out [20]. However, the transport properties of bilayer graphene which is irradiated by intense laser light have not been considered in much detail. Ryzhii *et al.* proposed that a phototransistor could be implemented using bilayer graphene [21], Wright *et al.* have found a large peak conductance in the terahertz and far infra-red frequency range for bilayer graphene nanoribbons [22], and we have previously suggested that valley-polarized electrons can be produced in gapped bilayer graphene [23].

In this paper, we give a comprehensive description of the band structure and density of states of irradiated bilayer graphene, both in zero external magnetic field and in a strong field. This is of fundamental physical importance, but also has application in the realm of devices and technology because of the growing consensus that graphene and its bilayer have vast potential in the fields of optoelectronics and photonics [4], and in the design of new electronic devices such as ambipolar transistors [24]. Also, the spin-like degrees of freedom in graphene (such as the lattice pseudospin and the valley) may allow for electronic implementations of the ideas of spintronics [25] which have been discussed in the literature [23, 26, 27, 28, 29]. In all of these areas, a thorough understanding of the basic properties of irradiated bilayer graphene is an essential building block for design and application of devices. In particular, this present work focuses on the generation of valley-polarized states which may be used as a filter for the generation of valley-polarized currents. This is an essential step in the realization of valley-tronics devices.

We briefly outline the structure of our paper. In Section 2 we describe the theoretical framework which we employ for both the zero-field and strong-field cases. Then we present and discuss the results of our calculations in Section 3 before summarizing and placing our work in the context of valley-tronic devices in Section 4. Various important formulae and derivations are collected in the Appendix.

## 2. Theoretical framework

The Hamiltonian of irradiated bilayer graphene is written as

$$\mathcal{H}(t) = H_0 + H_U + h(t)$$

where $H_0$ is the continuum limit of the tight binding Hamiltonian, $H_U$ describes the external electrostatic field due to a top gate or dopants, and $h(t)$ is the time-dependent part which depends only on the irradiating field. We take the nearest-neighbour approximation of this $H_0$, but in principle any combination of hopping terms can be included by computing the eigenfunctions of the static Hamiltonian numerically. The static part of the Hamiltonian $H_0 + H_U$ determines single particle wave functions $\varphi_X$, which span the spatial part of the Hilbert space of solutions of $\mathcal{H}(t)$ and which we shall use as a basis for the time-dependent solutions $\Psi(t)$ of $\mathcal{H}(t)$. The energy spectrum and wave functions of the static Hamiltonian are presented in Appendix A, both in zero external magnetic field and when a strong magnetic field quantizes the electron motion into Landau levels. The solutions of the time-dependent part are found via the Floquet theorem, which we describe below.

The time-dependent term in the Hamiltonian is not known *a priori*, so we describe the process by which it is derived. The irradiating field is represented as a time-dependent vector potential which is introduced to the static Hamiltonian via Peierl's substitution $\mathbf{p} \to \mathbf{p} + e\mathbf{A}$, where $e > 0$ is the magnitude of the electron charge. We write the vector potential as $\mathbf{A}(t) = [A_x(t), A_y(t)]$, and substituting into the static Hamiltonian in Equation (A.1) to find

$$h(t) = \xi v e \sigma_x \otimes \begin{pmatrix} 0 & A_x(t) - iA_y(t) \\ A_x(t) + iA_y(t) & 0 \end{pmatrix} \tag{1}$$

where $\sigma_x$ is the first Pauli matrix. The vector potential encodes all information about the radiation, such as the polarization of the light, strength of the field, and frequency of the radiation. In the case of linearly polarized light, this field can be represented as $\mathbf{A}_{\text{lin}} = A \cos \Omega_A t \, [\cos\theta, \sin\theta]$ where $\theta$ is the angle of polarization in the plane of the graphene and $\Omega_A$ is the frequency. The strength of the vector field is given by the parameter $A = F/\Omega_A$ where $F = |\mathbf{E}|$ is strength of the electric field. However, when the light is circularly polarized, there is a phase difference between the $x$ and $y$ components of the field so that

$$\mathbf{A}_{\pm} = A \, [\cos \Omega_A t, \pm \sin \Omega_A t] \tag{2}$$

where the plus or minus sign refer to right-handed and left-handed polarizations, respectively. Full details of the time-dependent Hamiltonians in each case are given in Appendix B.

It is not possible to develop exact solutions to the eigenvalue equation for $\mathcal{H}(t)$. However, since the pertubation $h(t)$ is periodic, we may employ the Floquet theorem [30] to write the full time-dependent wave function $\Psi(\mathbf{r}, t)$ as the product of a periodic function $\Phi(\mathbf{r}, t)$ (with period $t_0 = 2\pi/\Omega_A$) and a time evolution function. The 'temporal Brillouin zone' is the interval $0 < t < t_0$, and the wave function is

$$\Psi(\mathbf{r}, t) = e^{-i\varepsilon t/\hbar} \Phi(\mathbf{r}, t) \tag{3}$$

where $\Phi(\mathbf{r}, t + t_0) = \Phi(\mathbf{r}, t)$. The scalar constant $\varepsilon$ is called the quasienergy. This theorem is the temporal analogue of the Bloch theorem, so that the quasienergy is equivalent to the quasimomentum, and the time period is equivalent to the lattice constant of the reciprocal lattice. The periodic wave functions $\Phi$ are called 'Floquet states'. Substituting Equation (3) into the time-dependent Schrödinger equation yields $\mathcal{H}(t)\Phi(t) - i\hbar\frac{\partial}{\partial t}\Phi(t) = \varepsilon\Phi(t)$, an eigenvalue equation for the operator $\mathcal{F}(t) = \mathcal{H}(t) - i\hbar\frac{\partial}{\partial t}$ with $\mathcal{F}(t)\Psi(t) = 0$.

In order to solve the Schrödinger equation for $\mathcal{F}(t)$ and $\Phi(t)$, we consider an expanded Hilbert space $\mathcal{R} \otimes \mathcal{T}$ of square-integrable functions of space and functions

of time with period $t_0$ (see Ref. [31] for a full description). In this space, the scalar product is defined as the regular spatial scalar product with the average over one period:

$$\langle\langle n|m\rangle\rangle = \frac{1}{t_0}\int_0^{t_0} \langle n|m\rangle \, dt.$$

where $n$ and $m$ label arbitrary states in $\mathcal{R}\otimes\mathcal{T}$. Since the wave functions are periodic and the eigenfunctions of the static Hamiltonian $H_0 + H_U$ form a complete set for the spatial coordinates, we can write the wave functions as

$$\Phi_m(\mathbf{r},t) = \sum_{j,X} c_{jX}^m \bar{\Phi}_{jX}(\mathbf{r},t) \tag{4}$$

where $m$ labels the Floquet state and the Hilbert space $\mathcal{R}\otimes\mathcal{T}$ is spanned by the infinite set of functions

$$\bar{\Phi}_{jX}(\mathbf{r},t) = e^{ij\Omega_A t}\varphi_X(\mathbf{r})$$

such that $j \in \{\ldots,-2,-1,0,1,2,\ldots\}$, and $X$ labels the eigenstates of $H_0 + H_U$. The label $X$ contains all appropriate single-particle quantum numbers, but its exact composition depends on whether there is a magnetic field present in the system. The operator in Equation (1) does not couple states with different momenta, different spin, or which are in different valleys. Therefore the Floquet states which result from diagonalization of the $t$-dependent Hamiltonian retain these three quantities as good quantum numbers. The Hamiltonian can be written as a matrix by computing the matrix elements of $\mathcal{F}(t)$ over these states. This yields an infinite dimensional matrix which can be truncated for a sufficiently large number of terms in the Fourier expansion and numerically diagonalized to give quasienergies and wave functions to arbitrary precision. These matrix elements are discussed in Appendix B.

We now introduce the two-time formalism which we use to compute the Green's function and hence the density of states (DoS) in irradiated bilayer graphene. In this formalism, the time associated with the expanded Hilbert space (which was previously labelled '$t$' but which we shall call $\zeta$ from now on) is separated from the evolution of the system such that the full time-dependent solution of the Schrödinger equation $\Psi(\mathbf{r},t)$ is [30]

$$\Psi(\mathbf{r},t) = \Psi(\mathbf{r},\zeta,t)\Big|_{\zeta=t}. \tag{5}$$

The two-time wave function is then defined to be

$$\Psi(\mathbf{r},\zeta,t) = \exp\left(-\frac{i}{\hbar}\mathcal{F}(\zeta)(t-t')\right)\Psi(\mathbf{r},\zeta,t')$$

where $\mathcal{F}$ is the Floquet operator introduced earlier. Full time-dependent solutions are given by the limiting procedure in Equation (5), but we shall generally be interested in the dynamics of the system on timescales much longer than $t_0$ so we shall instead take the time average with respect to the field.

In the Matsubara formalism, we utilize the grand canonical ensemble, and define the associated energy scale $\kappa = \varepsilon - \mu$ where $\mu$ is the chemical potential. The operator for this energy is $\mathcal{K} = \mathcal{F} - \mu N$. The imaginary time $\tau = it$ is defined and the evolution of the field operators associated with the Floquet states is given by (the coordinate

dependence is implicit)

$$\psi(\zeta,\tau)=\sum_n e^{-\kappa_n\tau/\hbar}\Phi_n(\zeta)a_n, \tag{6}$$

$$\psi^\dagger(\zeta,\tau)=\sum_n e^{\kappa_n\tau/\hbar}\Phi_n^*(\zeta)a_n^\dagger, \tag{7}$$

where the index $n$ runs over all Floquet states. The Matsubara Green's function is

$$\mathcal{G}(\mathbf{r}\zeta,\mathbf{r}'\zeta',\tau-\tau')=\frac{-1}{\hbar}\mathrm{Tr}\left[e^{-\beta(\mathcal{K}-\Omega)}T_\tau\psi(\zeta,\tau)\psi^\dagger(\zeta',\tau')\right].$$

The operator $T_\tau$ is the $\tau$-ordering operator, $\Omega$ is the thermodynamic potential and serves as the normalizing factor for the thermodynamic average, and $\beta=1/(k_BT)$. The Fourier transform of this Green's function is the quantity from which the density of states can be calculated. The Fourier transform is

$$\mathcal{G}(\mathbf{p},i\omega_n)=\frac{1}{t_0^2}\int_0^{t_0}d\zeta\int_0^{t_0}d\zeta'\int_0^{\beta}d(\tau-\tau')e^{i\omega_n\tau}\times \\ \times\frac{1}{\mathcal{A}}\int d^2\mathbf{r}\int d^2\mathbf{r}'e^{i\mathbf{p}\cdot\mathbf{r}}e^{-i\mathbf{p}'\cdot\mathbf{r}}\mathcal{G}(\mathbf{r}\zeta\tau,\mathbf{r}'\zeta'\tau') \tag{8}$$

which includes an averaging procedure over the period of the fast oscillation associated with the radiation. The retarded Green's function $G^R$ can then be found by carrying out the analytic continuation $i\omega_n\to\omega+i\delta$ and the density of states can be extracted from this Green's function in the standard way:

$$\rho(\omega)=-\frac{1}{\pi}\mathrm{Im}\sum_{\mathbf{p}}\mathrm{tr}\,G^R(\mathbf{p},\omega) \tag{9}$$

where tr denotes the summation of the diagonal elements of $G^R$ which is a $4\times4$ matrix in the sublattice space.

## 3. Results

### *3.1. Zero magnetic field*

In the case of zero external magnetic field, the single particle quantum states in the system are of plane wave nature and are characterized by a two-dimensional wave vector $\mathbf{k}$. In addition, there are two (real) spins $\sigma$, two inequivalent valleys $\xi$, and four bands within each valley (labeled by the conduction or valence band $\nu$ and the high-energy or split branch $b$). The wave functions associated with these states are given in Appendix A.1. The energy spectrum is found by substituting the matrix elements of the radiation operator into the Hamiltonian and numerically diagonalizing the resulting matrix. The spectrum is shown in Figure 1. Panel (a) shows the unirradiated low energy bands for comparison with the other three plots. In zero magnetic field, the effective coupling parameter is $v_FeF/\hbar\Omega_A^2$ which implies that the strongest coupling occurs for smaller frequencies. This is illustrated by panels (b) and (c) which show the effects of an irradiating field with $\Omega_A=2\,\mathrm{THz}$ and $5\,\mathrm{THz}$ respectively with a field strength of $F=5\,\mathrm{kV\,cm^{-1}}$. The mixing between different Fourier harmonics is stronger for the lower frequency, but the dynamic gap opened by the mixing is larger for the higher frequency. The dynamic gaps only occur when states from opposite bands mix. States from the same band run parallel to each other (seperated in energy by $\hbar\Omega_A$) and therefore cannot cross. There is no gap at $k=0$ because the distribution

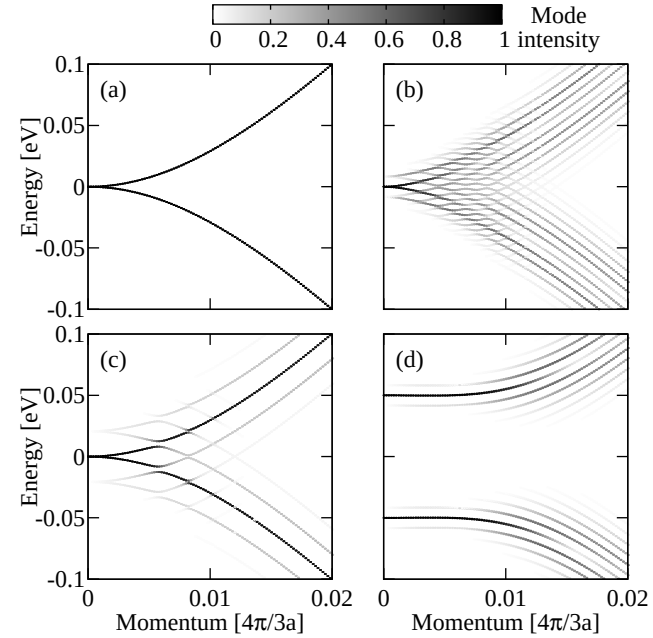



**Figure 1.** Energy spectrum of irradiated bilayer graphene in zero external magnetic field under right-handed circularly polarized light. (a) The unirradiated spectrum; (b) $\Omega_A = 2\,\mathrm{THz}$, $F = 5\,\mathrm{kV\,cm^{-1}}$; (c) $U = 100\,\mathrm{meV}$, $\Omega_A = 2\,\mathrm{THz}$, $F = 5\,\mathrm{kV\,cm^{-1}}$; (d) $\Omega_A = 5\,\mathrm{THz}$, $F = 5\,\mathrm{kV\,cm^{-1}}$.

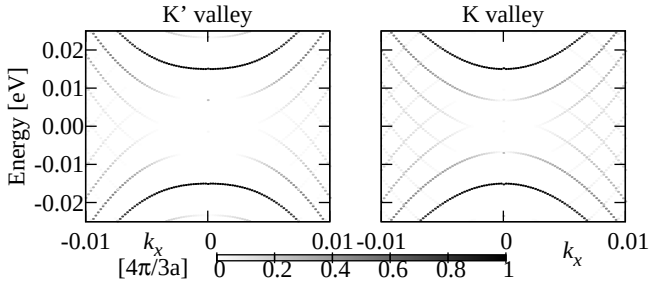



**Figure 2.** Valley asymmetry when interlayer bias potential is present. In these plots $F = 5\,\mathrm{kV\,cm^{-1}}$, $\Omega_A = 2\,\mathrm{THz}$, and $U = 30\,\mathrm{meV}$.

of the wavefunction across the four lattice sites forbids coupling for small momenta (see Appendix A).

When a gap is introduced to the spectrum by doping one side of the graphene bilayer or by electrostatic gating, the effect of the radiation is markedly different. This is because the gap means that consecutive Fourier harmonics from opposite bands do not cross, and therefore the spectral weight is spread only between Floquet states which originate from the same band. Therefore no anticrossings appear, although the effect of a broadening of the band will be seen. This is illustrated in panel (d) of Figure 1. However, as Figure 2 shows, the coupling to right-handed circularly polarized light is stronger in the K valley than in the K′ valley. This is due to the redistribution

of the wave function among the four lattice sites as a result of the interlayer bias potential which generates the gap. If the direction of the potential or the orientation of the irradiating field are changed, then the coupling becomes stronger in the K′ valley instead. If linearly polarized light is used, the response of electrons in the two valleys are identical since linearly polarized radiation can be represented as the sum of two circularly polarized components.

The Floquet wave functions which are calculated numerically can now be used in Equations (4) and (8) to compute the Green's function and hence the density of states. The Green's function is

$$G^R(\mathbf{p},\omega) = \frac{1}{\hbar}\sum_{n'} \frac{1}{\omega - \kappa_{\mathbf{p}n'}/\hbar + i\delta} \sum_x \left| c_{0x}^{\mathbf{p}n'} \right|^2$$

where $n'$ labels the discrete set of Floquet states with wave vector $\mathbf{p}$ and $x$ labels the unirradiated basis states with wave vector $\mathbf{p}$. The density of states can be calculated by substituting this expression into Equation (9) and numerically evaluating the integral over momentum:

$$\rho = \int_0^\Lambda p\,dp \sum_{x_\alpha} \frac{\delta}{\left(\hbar\omega - \kappa_\alpha\right)^2 + \delta^2} \sum_X |c_{0X}^{p\alpha}|^2$$

where $\Lambda$ is the momentum cut-off determined by requiring the summation over all states yields the correct electron density at half-filling. Plots of this function are shown in Figure 3. In (a), the interlayer bias potential is zero so that the graphene does not have a static gap. The density of states for unirradiated graphene is constant in this case, as predicted by straightforward analysis of the band structure. When the graphene is irradiated, dynamic gaps open at $\Omega_A/2$ and are clearly visible for stronger fields. The responses of electrons in the two valleys are identical. In (b), the same system parameters are used, except that now a small static gap is present ($U = 10\text{meV} = U/2$). In the unirradiated case (thin solid line), the static gap manifests as a region with near-zero DoS for small energies ($\hbar\omega < 5\text{meV}$). For $\hbar\omega > 5\text{meV}$, the dynamic gaps are still present. However, for $\hbar\omega < 5\text{meV}$, a finite DoS is present under strong radiation. This is due to the dynamical states that are induced by the radiation. In (c), the gap is wider ($U = 20\text{meV}$) and now the conduction and valence bands are seperated to an extent where significant coupling between them is not permitted. However, states within the same band do still couple causing the band edge to be significantly smeared and for electron density to be present in the static gap.

### *3.2. Quantizing magnetic field*

When a strong magnetic field is present in the system, the motion of the electrons is quantized into Landau levels. Using the Landau guage $\mathbf{A}_B = [0, Bx, 0]$, the discrete single particle quantum numbers are the same as in the zero field case, but the momentum is continuous in the $y$ direction and discrete in the $x$ direction. This is due to the gauge field which breaks the translational symmetry. Therefore, the sum over the two-dimentional momenta may be split into two separate one-dimensional sums, one discrete (over $k_x$) and the other represented by an integral with periodic boundary conditions (over $k_y$).

Figure 4 shows the evolution of the Landau level spectrum with increasing intensity of linearly polarized incident radiation. At $F = 0$, the standard bilayer

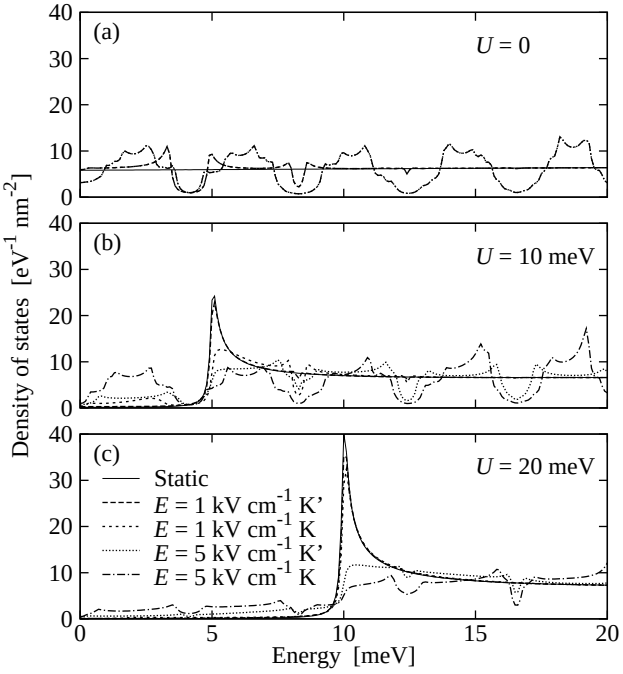



**Figure 3.** Density of states in bilayer graphene in zero magnetic field. (a) For ungapped bilayer graphene, the valley degeneracy is intact and gaps open at intervals of $\Omega_A/2 \approx 4.1\,\mathrm{meV}$. (b) $U = 10\,\mathrm{meV}$. A significant electron density is induced in the spectral gap by the radiation. (c) $U = 20\,\mathrm{meV}$. The spectral gap is too wide to allow significant coupling of electron and hole states.

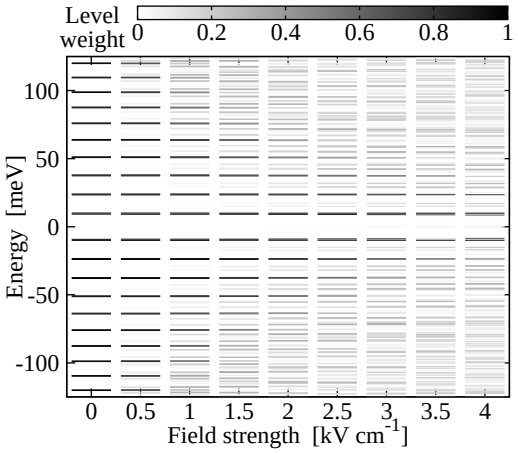



**Figure 4.** Evolution of energy levels with the strength of a linearly polarized irradiating field. The line thickness indicates the strength of the mode, $\Omega = 1\,\mathrm{THz}$, $U = 20\,\mathrm{meV}$, and $B = 5\,\mathrm{T}$. The spectrum of levels is symmetric about zero energy in this case.

Landau level spectrum is evident. For weak field, ($F < 1\,\mathrm{kV\,cm^{-1}}$) the mixing of dynamical states is small and the original Landau level spectrum is recognizable.

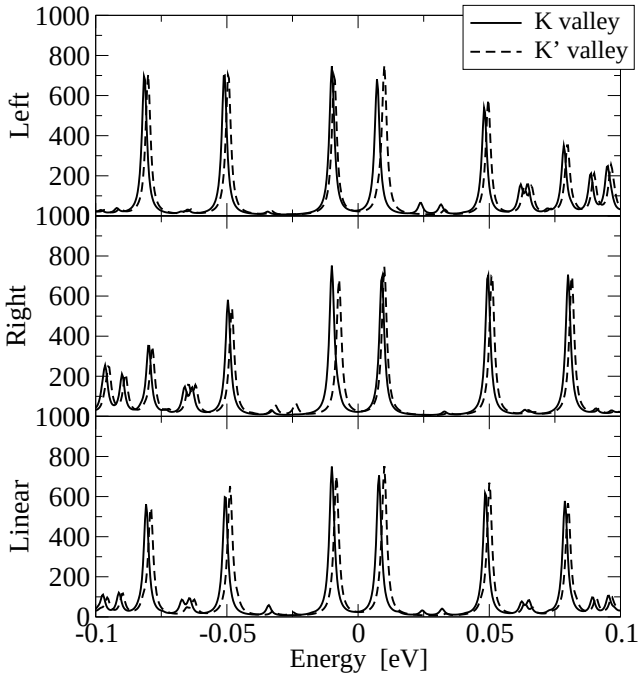



**Figure 5.** Density of states for $B = 12$T, $\Omega_A = 4\,\mathrm{THz}$, $U = 20$meV, and with $F = 5\,\mathrm{kV\,cm^{-1}}$ in each valley. The radiation shifts the energy of the Landau level, and coupling properties are different in the two bands.

For strong coupling ($F > 3\,\mathrm{kV\,cm^{-1}}$), the Landau level spectrum is replaced by a near-continuum of levels, each with rather small weight, and there are the beginings of states visible in the gapped region. Notice, however, that the two $\delta$-states barely change their intensity showing that they are only very weakly coupled to the radiation due to their unique distribution of wave function weight between the four sublattice sites.

The DoS in this case is evaluated using the same steps as in the zero magnetic field situation. The analytical expression which we must evaluate for the DoS is

$$\rho = \frac{\Lambda}{\pi\lambda_B}\sum_{x_\alpha}\frac{\delta}{\left(\hbar\omega - \kappa_\alpha\right)^2 + \delta^2}\sum_X |c_{0X}^\alpha|^2$$

This function is plotted in Figure 5 for bilayer graphene with a small inter-layer bias $U = 20$meV for left-handed, right-handed and linear polarization of the incident light. We clearly see the radiation-induced dynamical bands as expected. The first feature of these plots which requires discussion is the difference between the behavior in the conduction and valence bands for the two circular polarizations. This occurs because coupling between the radiation and the light and the electrons depends critically on the wave function components. The factors like $\xi\Xi \pm \varepsilon$ mean that the weight on each lattice component are different in the two bands, implying that the field will affect these electrons differently. When strong coupling occurs, the Landau level spectrum is almost washed out by the dynamical bands, but when coupling is weak, the states are still clearly discernable. There is also a slight shift in the energy of the Landau levels in each valley, which is caused by the broken valley degeneracy in the single-

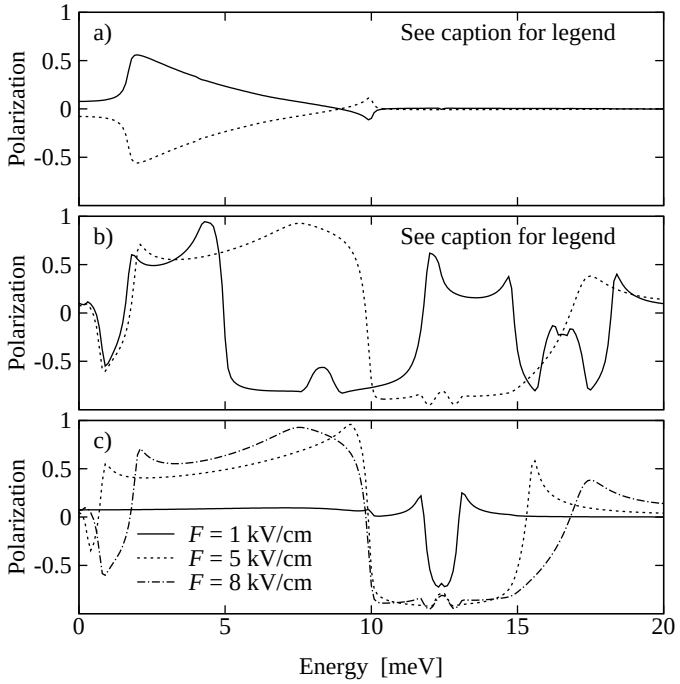



**Figure 6.** Valley polarization for zero magnetic field. a) Polarization for right-handed (solid line) and left-handed (dashed line) radiation with $\Omega_A = 2\,\mathrm{THz}$, $F = 1\,\mathrm{kV\,cm^{-1}}$, and $U = 20\mathrm{meV}$. b) Demonstration that polarization of almost unity can be achieved under specific conditions. Solid line has $\Omega_A = 4\,\mathrm{THz}$, $F = 5\,\mathrm{kV\,cm^{-1}}$ and $U = 10\mathrm{meV}$; Dashed line is $\Omega_A = 6\,\mathrm{THz}$, $F = 8\,\mathrm{kV\,cm^{-1}}$, and $U = 20\mathrm{meV}$. c) Polarization features caused by the dynamic spectral gaps at $\omega = \Omega_A/2$ become more pronounced with increasing field stength. In this panel, $\Omega_A = 6\,\mathrm{THz}$ and $U = 20\mathrm{meV}$.

particle spectrum [see Equation (A.3)]. The linear polarization shows this as a uniform downward shift of the Landau levels in the K valley relative to the K' valley.

## 4. Conclusions and summary

We have shown that under certain conditions, the coupling of electrons in biased bilayer graphene to the external electromagnetic field is not the same in either valley. In order to demonstrate how this might be applicable in the design of a device, we discuss how the existence of parameter ranges where there is significant DoS in one valley but not in the other allows us to consider the possiblity of generating valley-polarized electrons [23]. If a current is incident on a region of irradiated bilayer graphene where the radiation and inter-layer bias are tuned such that states only exist in one valley, then incident current in the valley where there are no states will not be able to traverse the irradiated region. This region can then act as a filter for the electron valley, leading to the possibility of switching devices and 'valleytronic' applications [23]. We define the polarization to be

$$\mathcal{P} = \frac{\rho_K - \rho_{K'}}{\rho_K + \rho_{K'}}$$

so that $\mathcal{P} = +1$ implies that all electrons are in the K valley and $\mathcal{P} = -1$ means that all are in the K' valley. Figure 6 shows the polarization for several different scenarios. Firstly, in panel a) we demonstrate that the left-handed and right-handed orientations of light induce polarization in opposite valleys. In panel b) we demonstrate that polarization can approach unity for specific values of the radiation parameters and bias potential. This is important if highly-polarized electron currents are to be produced. Lastly, in panel c) we show that the polarization induced near the dynamical gaps becomes more pronounced and exists for a wider energy range when the field strength is increased. This is in contrast to polarization features caused by additional dynamical states appearing in the static gap, which exist only for small parameter ranges. The features associated with the dynamical gaps also become stronger as the frequency $\Omega_A$ is increased.

In the case where a strong magnetic field is present, valley polarization may also be generated, but only as a result of the shift in energy of the Landau levels created by the radiation.

This work was supported by the Canada Research Chairs programme and the NSERC Discovery grant.

## Appendix A. Single particle description

We take the basis $\{\psi_{A_l}, \psi_{B_u}, \psi_{A_u}, \psi_{B_l}\}$ with $\xi = +1$ in the $K$ valley and the basis $\{\psi_{B_u}, \psi_{A_l}, \psi_{B_l}, \psi_{A_u}\}$ with $\xi = -1$ in the $K'$ valley so that the single particle nearest neighbour tight binding Hamiltonian for unbiased bilayer graphene can be written as [32]

$$H_0 = \begin{pmatrix} 0 & 0 & 0 & \xi v_F \pi^\dagger \\ 0 & 0 & \xi v_F \pi & 0 \\ 0 & \xi v_F \pi^\dagger & 0 & \gamma_1 \\ \xi v_F \pi & 0 & \gamma_1 & 0 \end{pmatrix}, \tag{A.1}$$

where $\pi = p_x + ip_y$ is the linear expansion of the transfer integral in the tight binding formalism, $\gamma_1$ is the energy of the inter-layer dimer bond, and $v_F$ is the Fermi velocity. Similarly, the inter-layer bias potential which sets the energy of lattice sites in the upper layer at $U/2$ and sites in the lower layer at $-U/2$ causes a gap of magnitude $U$ to open at the $K$ points, and is described in [33]

$$H_U = \begin{pmatrix} \xi U/2 & 0 & 0 & 0 \\ 0 & -\xi U/2 & 0 & 0 \\ 0 & 0 & -\xi U/2 & 0 \\ 0 & 0 & 0 & \xi U/2 \end{pmatrix}. \tag{A.2}$$

### *Appendix A.1. Zero magnetic field*

In the zero field case, the $\pi$ operators are constructed from the usual single-particle momentum operators $\pi = -i\hbar\partial_x - \hbar\partial_y$. The energy spectrum associated with the Hamiltonian $H_0 + H_U$ is

$$E_{\mathbf{k},\eta,b} = \nu \left( \frac{\gamma_1^2}{2} + \frac{U^2}{4} + \hbar^2 v_F^2 k^2 + b\sqrt{\frac{\gamma_1^4}{4} + \hbar^2 v_F^2 k^2 (U^2 + \gamma_1^2)} \right)^{\frac{1}{2}}$$

The quantum numbers $\nu = \pm 1$ and $b = \pm 1$ label the band and branch respectively. Henceforth, we denote the band and valley indices by the label $\alpha = \{\xi_\alpha, \nu_\alpha, b_\alpha\}$ to shorten the notation. The wave functions are given by

$$\varphi_{\mathbf{k},\alpha} = C_{\mathbf{k},\alpha}\frac{e^{i\mathbf{k}\cdot\mathbf{r}}}{\sqrt{\mathcal{A}}}\begin{pmatrix} \frac{\xi_\alpha\hbar v_F k e^{-i\theta_{\mathbf{k}}}}{\gamma_1}\frac{\xi_\alpha\Xi+E_{\mathbf{k},\alpha}}{\xi_\alpha\Xi-E_{\mathbf{k},\alpha}}f_{\mathbf{k},\alpha} \\ \frac{\xi_\alpha\hbar v_F k e^{i\theta_{\mathbf{k}}}}{\xi_\alpha\Xi+E_{\mathbf{k},\alpha}} \\ 1 \\ -\frac{\xi_\alpha\Xi+E_{\mathbf{k},\alpha}}{\gamma_1}f_{\mathbf{k},\alpha} \end{pmatrix}$$

$$f_{\mathbf{k},\alpha} = \frac{\hbar^2 v_F^2 k^2}{(\xi_\alpha\Xi + E_{\mathbf{k},\alpha})^2} - 1$$

$$C_{\mathbf{k},\alpha} = \left(\frac{\hbar^2 v_F^2 k^2}{(\xi_\alpha\Xi + E_{\mathbf{k},\alpha})^2} + 1 + \left[\frac{\hbar^2 v_F^2 k^2}{(\xi_\alpha\Xi - E_{\mathbf{k},\alpha})^2} + 1\right]\frac{(\xi_\alpha\Xi + E_{\mathbf{k},\alpha})^2}{\gamma_1^2}f_{\mathbf{k},\alpha}^2\right)^{-\frac{1}{2}}$$

where $\Xi = U/2$ and $\theta_{\mathbf{k}}$ is the angle of the wave vector $\mathbf{k}$ in the graphene plane.

*Appendix A.2. Quantizing magnetic field*

In this case, the $\pi$ operators are constructed from the guage-invariant momentum in a magnetic field found by making the minimal coupling substitution in the momentum operator so that $\mathbf{p} \to \mathbf{p} + e\mathbf{A}$. We label the Landau levels with a set of quantum numbers $\mathfrak{a} = \{n_\mathfrak{a}, \nu_\mathfrak{a}, \xi_\mathfrak{a}, q_\mathfrak{a}\}$ where $n > 0$ is the Landau level index, $\nu = +1(-1)$ in the conduction (valence) band, $\xi$ is the valley, and $q$ is the $x$ component of the wave vector which defines the guiding centre coordinate in the Landau gauge and we assume that all Landau levels are in the low-energy bands. Then, the Landau level energies $E_\mathfrak{a}$ are found by solving a polynomial equation derived using the Landau level operators $\pi\chi_n = -i\frac{\hbar\sqrt{2n}}{\lambda_B}\chi_{n-1}$ and $\pi^\dagger\chi_n = i\frac{\hbar\sqrt{2(n+1)}}{\lambda_B}\chi_{n+1}$:

$$\left[2(n_\mathfrak{a}+1) - (\Xi_{\xi_\mathfrak{a}} - E_\mathfrak{a})^2\right]\left[2n_\mathfrak{a} - (\Xi_{\xi_\mathfrak{a}} + E_\mathfrak{a})^2\right] \qquad -\gamma_1^2(\Xi_{\xi_\mathfrak{a}}^2 - E_\mathfrak{a}^2) = 0 \qquad \text{(A.3)}$$

where the energies are measured in units of $\hbar v_F/\lambda_B$ and $\Xi_\xi = \xi U/2$. The wave function associated with each Landau level is defined by the index of the Landau function in the third and fourth components. The $\chi$ functions are only defined for $n_\mathfrak{a} \geq 0$ so components of the $n_\mathfrak{a} = 0$ wave functions which contain indices outside of this range have zero weight on those components. The wave functions are:

$$\varphi_\mathfrak{a} = \frac{d_\mathfrak{a}e^{ik_\mathfrak{a}y}}{\sqrt{L\lambda_B\sqrt{\pi}}}\begin{pmatrix} \frac{-i\xi_\mathfrak{a}\sqrt{2(n_\mathfrak{a}+1)}}{\Xi_{\xi_\mathfrak{a}} - E_\mathfrak{a}}g_\mathfrak{a}\chi_{n_\mathfrak{a}+1}(r_\mathfrak{a}) \\ \frac{-i\xi_\mathfrak{a}\sqrt{2n_\mathfrak{a}}}{\Xi_{\xi_\mathfrak{a}} + E_\mathfrak{a}}\chi_{n_\mathfrak{a}-1}(r_\mathfrak{a}) \\ \chi_{n_\mathfrak{a}}(r_\mathfrak{a}) \\ g_\mathfrak{a}\chi_{n_\mathfrak{a}}(r_\mathfrak{a}) \end{pmatrix} \equiv \frac{d_\mathfrak{a}e^{ik_\mathfrak{a}y}}{\sqrt{L\lambda_B\sqrt{\pi}}}\begin{pmatrix} \mathfrak{w}_\mathfrak{a}\chi_{n_\mathfrak{a}+1}(r_\mathfrak{a}) \\ \mathfrak{x}_\mathfrak{a}\chi_{n_\mathfrak{a}-1}(r_\mathfrak{a}) \\ \mathfrak{y}_\mathfrak{a}\chi_{n_\mathfrak{a}}(r_\mathfrak{a}) \\ \mathfrak{z}_\mathfrak{a}\chi_{n_\mathfrak{a}}(r_\mathfrak{a}) \end{pmatrix}$$

$$d_\mathfrak{a} = \left[\left(\frac{2(n_\mathfrak{a}+1)}{(\xi_\mathfrak{a}\Xi - E_\mathfrak{a})^2} + 1\right)g_\mathfrak{a}^2 + \frac{2n_\mathfrak{a}}{(\xi_\mathfrak{a}\Xi + E_\mathfrak{a})^2} + 1\right]^{-\frac{1}{2}},$$

$$g_\mathfrak{a} = \frac{1}{\gamma_1}\frac{1}{\xi_\mathfrak{a}\Xi + E_\mathfrak{a}}\left[(\xi_\mathfrak{a}\Xi + E_\mathfrak{a})^2 - 2n_\mathfrak{a}\right],$$

with $r_\mathfrak{a} = x/\lambda_B - q_\mathfrak{a}\lambda_B$ and

$$\chi_{n_\mathfrak{a}}(r_\mathfrak{a}) = \frac{1}{\sqrt{n_\mathfrak{a}!2^{n_\mathfrak{a}}}}e^{-r_\mathfrak{a}^2/2}H_{n_\mathfrak{a}}(r_\mathfrak{a})$$

In addition to these functions, there are also two '$\delta$-states' with energy $\pm U/2$ which account for the doubled degeneracy of the zero energy Landau levels in unbiased bilayer graphene. The wave functions of these states are

$$\varphi_{\delta\mathfrak{a}} = \frac{e^{ik_{\mathfrak{a}}y}}{\sqrt{L\lambda_B\sqrt{\pi}}} \begin{pmatrix} \chi_0(r_{\mathfrak{a}}) \\ 0 \\ 0 \\ 0 \end{pmatrix}$$

## Appendix B. Matrix elements of $\mathcal{F}(\tau)$

For convenience, we restate the definition of $\mathcal{F}(\tau) = \mathcal{H}(\tau) - i\hbar\frac{\partial}{\partial\tau} = H_0 + H_U + h(\tau) - i\hbar\frac{\partial}{\partial\tau}$. The matrix elements contain several terms. The terms relating to the static Hamiltonian and the time derivative are

$$\langle\langle j'X'|H_0 + H_U - i\hbar\frac{\partial}{\partial\tau}|jX\rangle\rangle = (E_X + j\hbar\Omega_A)\,\delta_{j,j'}\delta_{X,X'}$$

The matrix elements of the term associated with the irradiating field $h(\tau)$ depend on the specific nature of the field and the wave functions. For example, linearly polarized light can be described by the vector potential $\mathbf{A}_{\rm lin}(\tau) = A\cos(\Omega\tau)\,[\cos\theta, \sin\theta]$ where $\theta$ is the angle of polarization in the plane of the graphene with respect to the $x$ axis. This yields

$$h_{\rm lin}(\tau) = \frac{\xi v_F eF}{\Omega_A}\sigma_x \otimes \begin{pmatrix} 0 & e^{i\theta} \\ e^{-i\theta} & 0 \end{pmatrix} \cos(\Omega_A\tau).$$

Since we discuss radiation incident at the perpendicular to the graphene plane, this angle is immaterial and we can substitute $\theta = 0$ without loss of generality. On the other hand, circularly polarized light is given by $\mathbf{A}_{\pm}(\tau) = A\,[\cos(\Omega_A\tau), \pm\sin(\Omega_A\tau)]$ where the positive or negative sign corresponds to right- or left-handed orientations of the polarization:

$$h_{\pm}(\tau) = \frac{\xi v_F eF}{\Omega_A}\sigma_x \otimes \begin{pmatrix} 0 & e^{\mp i\Omega_A\tau} \\ e^{\pm i\Omega_A\tau} & 0 \end{pmatrix}$$

### *Appendix B.1. Zero magnetic field*

In this case the matrix elements of linearly polarized light (taking $\theta = 0$) are zero for states with unequal wave vectors, and as follows for states in the same valley and with the same spin, which also have identical wave vector $\mathbf{k}$:

$$\langle\langle j'\mathbf{k}\alpha'|h_{\rm lin}(\tau)|j\mathbf{k}\alpha\rangle\rangle = \frac{\hbar v_F^2 keF}{2\Omega}\left(\delta_{j',j+1} + \delta_{j',j-1}\right) C_\alpha C_{\alpha'}\delta_{\xi,\xi_\alpha}\delta_{\xi,\xi_{\alpha'}} \times$$
$$\times\left[\frac{e^{-i\theta_{\mathbf{k}}}}{\xi\Xi + E_{\alpha'}} + \frac{e^{i\theta_{\mathbf{k}}}}{\xi\Xi + E_\alpha} - \frac{f_\alpha f_{\alpha'}}{\gamma_1^2}\left(\xi\Xi + E_{\alpha'}\right)\left(\xi\Xi + E_\alpha\right)\left(\frac{e^{i\theta_{\mathbf{k}}}}{\xi\Xi - E_{\alpha'}} + \frac{e^{-i\theta_{\mathbf{k}}}}{\xi\Xi - E_\alpha}\right)\right].$$

The matrix elements of states with different spin or valley are zero. Similarly, the matrix elements of the Hamilonian associated with circularly polarized radiation are diagonal in the wave vector, spin, and valley and are given by

$$\langle\langle j'\mathbf{k}X'|h_{\pm}(\tau)|j\mathbf{k}X\rangle\rangle = \frac{\hbar v_F^2 keF}{\Omega} C_X C_{X'}\delta_{\xi,\xi_X}\delta_{\xi,\xi_{X'}} \times$$
$$\times\left\{\delta_{j',j\mp1}e^{i\theta_{\mathbf{k}}}\left[\frac{1}{\xi\Xi + E_\alpha} - \frac{f_\alpha f_{\alpha'}}{\gamma_1^2}\frac{(\xi\Xi + E_{\alpha'})(\xi\Xi + E_\alpha)}{\xi\Xi - E_{\alpha'}}\right] + \right.$$
$$\left. + \delta_{j',j\pm1}e^{-i\theta_{\mathbf{k}}}\left[\frac{1}{\xi\Xi + E_{\alpha'}} - \frac{f_\alpha f_{\alpha'}}{\gamma_1^2}\frac{(\xi\Xi + E_\alpha)(\xi\Xi + E_{\alpha'})}{\xi\Xi - E_\alpha}\right]\right\}.$$

*Appendix B.2. Quantizing magnetic field*

The matrix elements in this case are

$$\langle\langle j'\mathfrak{a}'|h_{\rm lin}(\tau)|j\mathfrak{a}\rangle\rangle = \frac{iv_F eF}{\sqrt{2}\Omega}\left(\delta_{j',j+1}+\delta_{j',j-1}\right) d_{\mathfrak{a}}d_{\mathfrak{a}'}\delta_{k_{\mathfrak{a}},k_{\mathfrak{a}'}}\delta_{\xi,\xi_{\mathfrak{a}}}\delta_{\xi,\xi_{\mathfrak{a}'}}\times$$
$$\times\Bigg\{\delta_{n_{\mathfrak{a}},n_{\mathfrak{a}'}+1}\sqrt{n_{\mathfrak{a}}}\left(\frac{g_{\mathfrak{a}}g_{\mathfrak{a}'}}{\xi\Xi-E_{\mathfrak{a}'}}-\frac{1}{\xi\Xi+E_{\mathfrak{a}}}\right)$$
$$-\delta_{n_{\mathfrak{a}},n_{\mathfrak{a}'}-1}\sqrt{n_{\mathfrak{a}}+1}\left(\frac{g_{\mathfrak{a}}g_{\mathfrak{a}'}}{\xi\Xi-E_{\mathfrak{a}}}-\frac{1}{\xi\Xi+E_{\mathfrak{a}'}}\right)\Bigg\},$$

and

$$\langle\langle j'\mathfrak{a}'|h_{\pm}(\tau)|j\mathfrak{a}\rangle\rangle = \frac{\sqrt{2}iveF}{\Omega}d_{\mathfrak{a}}d_{\mathfrak{a}'}\delta_{k_{\mathfrak{a}},k_{\mathfrak{a}'}}\delta_{\xi,\xi_{\mathfrak{a}}}\delta_{\xi,\xi_{\mathfrak{a}'}}\times$$
$$\times\Bigg\{\delta_{j',j\mp1}\delta_{n'_{\mathfrak{a}},n_{\mathfrak{a}-1}}\sqrt{n_{\mathfrak{a}}}\left(\frac{g_{\mathfrak{a}}g_{\mathfrak{a}'}}{\xi\Xi-E_{\mathfrak{a}'}}-\frac{1}{\xi\Xi+E_{\mathfrak{a}}}\right)$$
$$-\delta_{j',j\pm1}\delta_{n_{\mathfrak{a}'},n_{\mathfrak{a}+1}}\sqrt{n_{\mathfrak{a}}+1}\left(\frac{g_{\mathfrak{a}}g_{\mathfrak{a}'}}{\xi\Xi-E_{\mathfrak{a}}}-\frac{1}{\xi\Xi+E_{\mathfrak{a}'}}\right)\Bigg\}.$$


[1] K. S. Novoselov, A. K. Geim, S. V. Morozov, D. Jiang, Y. Zhang, S. V. Dubonos, I. V. Grigorieva, and A. A. Firsov, Science **306**, 666 (2004).
[2] T. Ohta, A. Bostwick, T. Seyller, K. Horn, and E. Rotenberg, Science **313**, 951 (2006);
[3] For a full review of the physics of graphene, see D. S. L. Abergel, V. Apalkov, J. Berashevich, K. Ziegler, and Tapash Chakraborty, Adv. Phys. **59**, 261 (2010)
[4] F. Bonaccorso, Z. Sun, T. Hasan, and A. C. Ferrari, Nat. Photon. **4**, 611 (2010).
[5] N. Stander, B. Huard, and D. Goldhaber-Gordon, Phys. Rev. Lett. **102**, 026807 (2009).
[6] A. F. Young, and P. Kim, Nat. Phys. **5**, 222 (2009).
[7] K. S. Novoselov, A. K. Geim, S. V. Morozov, D. Jiang, M. I. Katsnelson, I. V. Grigorieva, S. V. Dubonos, and A. A. Firsov, Nature **438**, 197 (2005).
[8] Y. Zhang, Y.-W. Tan, H. L. Stormer and P. Kim, Nature **438**, 201 (2005).
[9] J. B. Oostinga, H. B. Heersche, X. Liu, A. F. Morpurgo, and L. M. K. Vandersypen, Nat. Mater. **7**, 151 (2008).
[10] F. T. Vas'ko and V. Ryzhii, Phys. Rev. B **77**, 195433 (2008).
[11] A. Satou, F. T. Vasko, and V. Ryzhii, Phys. Rev. B **78**, 115431 (2008).
[12] López-Rodríguez and G. G. Naumis, Phys. Rev. B **78**, 201406(R) (2008).
[13] S. A. Mikhailov and K. Ziegler, J. Phys. Condens. Matter **20**, 384204 (2008).
[14] A. R. Wright, X. G. Xu, J. C. Cao, and C. Zhang, Appl. Phys. Lett. **95**, 072101 (2009).
[15] T. Oka, and H. Aoki, Phys. Rev. B **79**, 081406(R) (2009).
[16] J. Liu, A. R. Wright, C. Zhang, and Z. Ma, Appl. Phys. Lett. **93**, 041106 (2008).
[17] Jun-Qiang Lu, X.-G. Zhang, and Sokrates T. Pantelides, Phys. Rev. B **79**, 073408 (2009).
[18] M. V. Fistul and K. B. Efetov, Phys. Rev. Lett. **98**, 256803 (2007).
[19] S. V. Syzranov, M. V. Fistul, and K. B. Efetov, Phys. Rev. B **78**, 045407 (2008).
[20] H. Choi, F. Borondics, D. A. Siegel, S. Y. Zhou, M. C. Martin, A. Lanzara, and R. A. Kaindl, Appl. Phys. Lett **94**, 172102 (2009).
[21] V. Ryzhii and M. Ryzhii, Phys. Rev. B **79**, 245311 (2009).
[22] A. R. Wright, J. C. Cao, and C. Zhang, Phys. Rev. Lett. **103**, 207401 (2009).
[23] D. S. L. Abergel and T. Chakraborty, Appl. Phys. Lett. **95**, 062107 (2009).
[24] X. Yang, G. Liu, A. A. Balandin, and K Mohanram, ACS Nano **4**, 5532 (2010).
[25] I. Žutić, J. Fabian, and S. Das Sarma, Rev. Mod. Phys. **76**, 323 (2004).
[26] A. Rycerz, J. Tworzydło, and C. W. J Beenakker, Nat. Phys **3**, 172 (2007).
[27] D. Xiao, W. Yao, and Q. Niu, Phys. Rev. Lett. **99**, 236809 (2007).
[28] I. Martin, Ya. M. Blanter, and A. F. Morpurgo, Phys. Rev. Lett. **100**, 036804 (2008).
[29] J. L. Garcia-Pomar, A. Cortijo, and M. Nieto-Vesperinas, Phys. Rev. Lett. **100**, 236801 (2008).
[30] T. Dittrich, P. Hänggi, G.-L. Ingold, B. Kramer, G. Schön, and W. Zwerger, *Quantum Transport and Dissipation*, (Wiley, Weinheim, 1998), Chap. 5.
[31] H. Sambe, Phys. Rev. A **7**, 2203 (1973).
[32] E. McCann and V. I. Fal'ko, Phys. Rev. Lett. **96**, 086805 (2006).
[33] E. McCann, Phys. Rev. B **74**, 161403(R) (2006).